Chapter 8

PHOTOVOLTAIC - ELECTROLYSIS CELLS

8.1 Introduction

Steam reforming of methane is currently the most common method of producing hydrogen and, as a by-product, CO_2,

a) $CH_4 + H_2O \rightarrow CO + 3H_2$
b) $CO + H_2O \rightarrow H_2 + CO_2$

which does the world no favors with respect to issues of global warming. As discussed in Chapter 2 water electrolysis is another way to produce hydrogen, however the electricity we use today is predominately obtained by the combustion of the fossil fuels that, like methane, are of finite supply and produce as a combustion product CO_2 as well as other noxious pollutants such as mercury vapor.

Electricity generated from sunlight offers a viable pathway for hydrogen production by water electrolysis [1-34], see **Fig. 8.1**, with photovoltaics (solar cells) converting solar energy into the electric energy needed to achieve water electrolysis resulting in the production of very pure hydrogen. Solar cells are commonly referred to as *photovoltaic* (PV) cells; *Photo* (light) and *Voltaic* (electricity). Several review articles consider the characteristics and performance of such systems, comprised of a photovoltaic converter and electrolysis device [5,6,9,16,17,19,21,29]. The global efforts at developing thin-film solar cell technology over the past decade, moving towards low-cost (plentiful) raw materials for their manufacture coupled with inexpensive (low energy input) mass production techniques, suggest that electricity from PV systems (and therefore PV hydrogen) should become increasingly less costly. The

'less costly' equation becomes particularly meaningful when the true costs of fossil fuels are factored into the equation, e.g. the military costs spent on ensuring oil flow from the Middle East, the associated political bargains necessarily made to keep the oil flowing, pollution and their associated medical affects, and of course the consequences of undesired global climate change.

Solar cells are silent, have no moving parts, cause no environmental pollution in operation, can generate power locally where it is needed, and can operate across extensive temperature regimes. Devices combining photovoltaic solar cells and water electrolysis may be described as integrated, or monolithic, tandem PV-electrolytic devices [35-39]. Multiple bandgap PV devices lead to a more efficient conversion of solar energy, hence a greater production of hydrogen [35-45] but at greater cost.

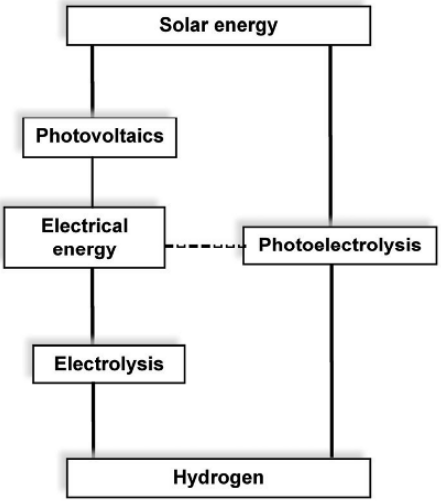

Fig. 8.1: Photovoltaic cell in combination with water electrolysis device for producing solar hydrogen.

8.2 General Description of Solar Cell Technology

8.2.1 From Past to Present

The recorded development of solar cell technology begins with the 1839 research of French experimental physicist Antoine-Edmond Becquerel [46,47]. At the age of nineteen he discovered the

photovoltaic effect while experimenting with an electrolytic cell containing two metal electrodes. He found that certain metals and solutions would produce small amounts of electric current when exposed to light. In 1883 Charles Fritts formed photovoltaic junctions by coating selenium with an extremely thin layer of gold [48]. Russell Ohl invented the first silicon solar cell in 1941 [49]. The era of modern solar cell technology began in 1954, when G. L. Pearson, D. Shapin and C. Fuller demonstrated a silicon solar cell capable of 6% energy conversion efficiency with direct sunlight [50]. The first gallium arsenide (GaAs) solar cell was reported in 1956, with a photoconversion efficiency of 6.5% [51]. In 1976 Carlson and Wronksi [52-54] reported solar cells comprised of amorphous silicon. Modern multi-junction solar cells can be viewed as a series of p-n junction photodiodes, each of different bandgap, that commonly include such III-V or II-VI materials as gallium arsenide (GaAs), gallium indium phosphide (GaInP), copper indium diselenide (CIS), copper indium-gallium diselenide (CIGS), and cadmium telluride (CdTe). In 1987, Jerry Olson [55-57] reported a two-junction tandem photovoltaic device consisting of an upper GaInP layer and lower GaAs layer, with a photoconversion efficiency up to 29.5% under concentrated solar light. The addition of a third junction further increases the conversion efficiency, to 34% for a GaInP/GaAs/Ge solar cell [58], to 40% for a GaInP/GaAs/GaInAs cell [59,60]. It is believed that the photoconversion efficiency of multi- (or many) junction solar cells can be increased up to 55% [61]. For example, highly mis-matched alloys such as $Zn_{1-y}Mn_yO_xTe_{1.x}$ have shown utility in the high performance high dollar solar cell markets, such as in space satellites, where dollars are no issue but high photoconversion efficiency is [62]. Unfortunately issues of cost limit application of solar cell technology in the 'real' world. The solar cell market continues to be dominated by silicon, the fabrication of which is energy-intensive requiring a manufacturing energy input equal to several years of energy output of the solar device. Furthermore modest device [63,64] efficiencies correspond to large land area requirements to meet the intrinsic energy demands of modern society. Generally speaking, as of today the cost of energy from solar cells is ≈ five times that produced by the burning of fossil

fuels. However since fossil fuels are freely provided by nature, and still so cheap as to be commonly treated as free (and not treated as an irreplaceable precious commodity), the factor of five looks pretty modest.

Following M. A. Green [65], 3rd generation photovoltaic solar cells refer to any device that exceeds the efficiency of a single junction solar cell, including the well-known tandem solar cells as well as other approaches that may, for example, circumvent previous assumptions such as one quasi-Fermi level separation existing in a solar cell, one photon generating one electron-hole pair, or a constant temperature existing across the device, etc., giving an approach or pathway to high device efficiencies such as: (A) Multiple absorption path solar cells, in which the absorption process is altered such that either two (low-energy) photons are absorbed to create a single electron-hole pair or alternately one photon creates multiple electron-hole pairs. (B) Multiple spectrum solar cells, where the solar spectrum is changed into a different spectrum with the same energy. (C) Multiple temperature solar cells, which involve the extraction of energy from variations in either carrier or lattice temperature. (D) Multiple energy level solar cells, which have more than a single quasi-Fermi level separation.

8.2.2 Operational Principles

On earth, as opposed to outer space, the most common solar cell material is silicon. An atom of silicon has 14 electrons, arranged in three different shells, $1s^2 2s^2 2p^6 3s^2 3p^2$. The first two shells are full, while the outer shell is half full, hence there are four electrons a silicon atom can and does share with its neighboring atoms. Pure silicon is a poor conductor of electricity since none of its electrons are free to move about.

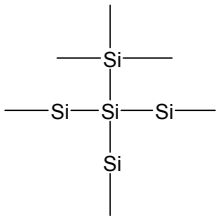

Intrinsic silicon

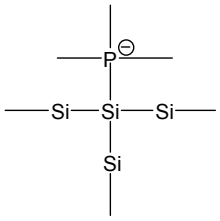

n-type silicon

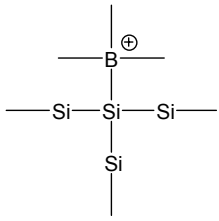

p-type silicon

When a Si atom is replaced with a Column V atom (e.g. P or As), there is an electron more than that which can be bonded through nearest neighbor associations. Relatively little energy is required to manipulate this extra electron; the resulting silicon is called **n-type** (*n* for negative net charge). When silicon is doped with a group III atom (e.g. B or Al), which have only three electrons in their outer shells the result is **p-type** silicon (*p* for positive net charge). The absence of an electron is considered a hole that carries positive charge. When p-type Si is adjacent to n-type Si the concentration gradients result in diffusion of the holes from the p-type side into the n-type side, and diffusion of electrons from the n-side into the p-side. The uncompensated charge result in an electric field across this space charge region that serves to separate any electrons and holes created by photon absorption, see **Fig. 8.2**; the electric field will send the electron to the n-side and the hole to the p-side. This causes further disruption of charge neutrality, and if an external current path is provided electrons will flow through the path to the p-side to unite with the holes the electric field sent there, doing useful work along the way. The electron flow provides the current, and the electric field of the junction provides the voltage; with current and voltage we have power.

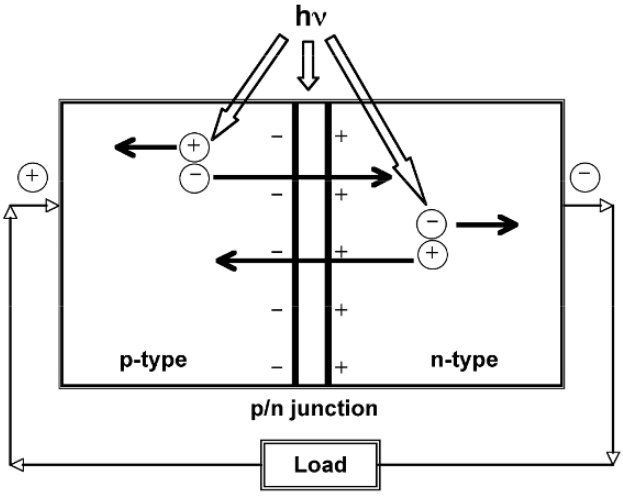

Fig. 8.2: Operation mechanism of single-crystal silicon p/n junction solar cell.

8.2.3 Crystalline Silicon Solar Cells

Since silicon accounts for the large majority of terrestrial solar cells we briefly consider some of their design issues. To minimize series resistance good electrical contacts are of critical importance, commonly achieved by covering the bottom with a metal film contact, and on the top using a transparent conductor such as SnO_2 or metallic contact grid that reduces the distance traveled by the photogenerated electrons while covering only a small part of the cell surface, see **Fig. 8.3**. Antireflection coatings, such as silicon monoxide (SiO_x) or silicon nitride (SiN_x), are used to minimize surface reflections without which silicon will reflect more than 30% of the incident light. Texturing of the surface by selective etching can also be used to reduce reflection. To protect the cell from the environment the cell is covered with a glass plate. PV modules are made by connecting several cells in series or parallel to achieve useful levels of voltage and current, and putting them in a sturdy frame complete with a glass cover and electrical terminals.

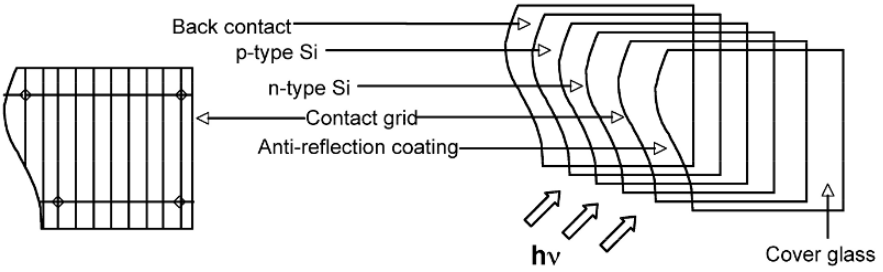

Fig. 8.3: Generic design of single-crystalline solar cell.

8.2.4 Types of Solar Cells

Single crystal silicon (sc-Si), polycrystalline silicon (p-Si), and amorphous silicon (a-Si) can all be used to make solar cells, with fabrication cost and device photoconversion efficiencies decreasing as one moves from single-crystal to amorphous materials. Various properties of these materials are summarized in **Table 8.1**. Other relatively common solar cell materials include gallium arsenide (GaAs), copper indium diselenide (CIS), copper indium-gallium

diselenide (CIGS), and cadmium telluride (CdTe). Amorphous silicon is one of the most developed thin film technologies to-date, and offers interesting possibilities in further development through the use of "microcrystalline" silicon which seeks to combine the stable high efficiencies of crystalline Si technology with the simpler and cheaper large area deposition technology of amorphous silicon. However different semiconductor materials, or combinations thereof, are only suited for responding to a specific spectral range. Therefore for a given semiconductor a portion of the radiant energy spectra cannot be used because some of the light quanta will not have enough energy to activate the charge carriers, and some of the light quanta will have surplus amounts of energy that will be transformed into heat rather than electrical energy. There are also optical losses due to reflection, or shadowing of the cell surface. Other losses occur due to the electrical resistances of the semiconductor and connecting cables. Losses intrinsic to a semiconductor photovoltaic include material contamination, surface effects, and crystal defects. Loss mechanisms associated with a bandgap lead to a theoretical maximum efficiency, which in the case of sc-silicon is approximately 33%. The efficiency of a solar cell is calculated by:

$$\eta_{global} = \frac{V_{OC} \times J_{SC} \times FF}{I_S}$$

where V_{oc} represents open circuit voltage, J_{sc} short-circuit current density, FF the fill factor, and I_s the power of the incident light. The fill factor is the ratio of solar cell's actual power to that obtained from its J_{SC} and V_{OC} values.

Table 8.1: Description of silicon based PV solar cells and their efficiencies.

Types	Crystal size range	Deposition method	Laboratory efficiency (%)	Production efficiency (%)
Single-crystal silicon, sc-Si	10-15 cm	Czochralski, Float Zone	~25	21.8
Multi-crystalline silicon, mc-Si	< 10 cm	Sawing (Cast)	~20	18.1
Polycrystalline silicon, p-Si	≈ 1mm	Chemical Vapor Deposition	~18	15.0
Amorphous, a-Si (Microcrystalline silicon)	(< 1mm)	Plasma Deposition	~13	7.0

Solar cells are broadly classified into five types based on their intrinsic structures, that we now briefly consider.

Homojunction

Selective doping alters a single semiconducting material to form within it a p-n junction. Single-crystal or multi-crystalline silicon are the most common examples of this type of cell, with other examples including GaAs and InP, see **Table 8.2**. In order to improve conversion efficiency various design aspects can be considered and varied such as material purity and crystallinity, depth of the p/n junction below the materials surface, and amount and distribution of dopant atoms on either side of the p/n junction.

Heterojunction

Hetero-junction devices are comprised of two different semiconductors. The top, or window, layer uses a material of higher bandgap while the bottom layer uses a material of lower bandgap. Thin-film p-CdTe|n-CdS solar cells are one such promising hetero-junction device, see **Table 8.2**. The 2.4 eV bandgap of CdS makes it transparent down to a wavelength of 515 nm. The p-CdTe layer (bandgap = 1.5 eV) is doped less than that of the n-CdS layer, hence the depletion region is mostly within the p-CdTe layer. Consequently most of the carrier generation and collection occurs within the p-CdTe layer, with ≈ 99% of the incident light absorbed by a 1 μm layer (compared with ≈ 10 μm for Si).

Table 8.2: Various solar cells (modules) and their efficiencies at global AM 1.5 spectrum (1000 W/m^2) [10]

Classification	Efficiencies (%)	Classification	Efficiencies (%)
III-V		**Multi-junction (tandem cell)**	
GaAs(Crystalline)	25.1	GaInP/GaAs	30.3
GaAs (thin film)	24.5	GaInP/GaAs/Ge	32.0
GaAs (Multi-crystalline)	18.2	GaAs/CIS	25.8
InP (crystalline)	21.9	a-Si/μC-Si	11.7
Thin film		GaInP/GaInAs/Ge	31.3
CdTe (thin film cell)	16.5	a-Si/a-Si/a-SiGe	12.1
CdTe (thin film submodule)	10.6	AlGaAs/GaAs	28.6
CIGS (thin film cell)	18.4	**Concentrator Cell**	
CIGS (thin film submodule)	16.6	GaInP/GaAs/Ge	34.7
GaAs (thin film cell)	24.5	GaInP/GaInAs/Ge	39.0
		GaAs (single cell)	27.8
		Si (single cell)	26.8
		CIGS (film, single cell)	21.5
		InP (single cell)	25.3

p-i-n Devices

These devices consist of a three-layer stack, with an intrinsic (i-type or undoped) layer between a n-type layer and p-type layer. This geometry results in an electric field between the p- and n-type regions that stretches across the resistive intrinsic region. Each photon absorbed in the intrinsic layer generates an electron-hole pair that is then separated by the electric field. In 1977 Carlson reported an amorphous silicon (a-Si) solar cell with a photoconversion efficiency of 5.5%, produced by glow-discharge decomposition of silane [66]. Twenty years later, Yang and co-workers reported an amorphous silicon p-i-n device with a photoconversion efficiency of 13% [67]. It was first shown by Guha et al. [68] that hydrogen dilution of the active gas mixture during deposition of the amorphous silicon thin films can be used to improve material quality (hydrogenated amorphous silicon, a-Si:H). The promise of a-Si:H solar cells is currently incomplete because of the light induced photo-degradation of its electronic properties known as the Staebler-Wronski effect [69]. As the hydrogen dilution is increased, the transition from amorphous to microcrystalline phase takes place; recent work has shown that the best amorphous silicon alloy is grown at a dilution just below the edge of amorphous to the microcrystalline (μc) transition (μc-Si:H) [70-72]. Materials such as Ge, B, and N have been used to form amorphous silicon alloys to obtain higher open circuit voltages.

Since a-Si:H holes have limited mobility relative to that of electrons, the devices are designed so that light enters through the p-layer to enable efficient hole collection [72], see **Fig. 8.4**. a-Si:H differs from crystalline silicon by the lack of long range order and the high (bonded) hydrogen content (~10% in device quality a-Si:H), with a key feature of this material its relative stability to light induced photodegradation. Although the overall properties of a-Si:H and sc-Si materials are similar due to similarities in short range order, the long range disorder in a-Si:H results in bond length and bond angle distortions, bond defects and microvoids. The major deposition variables in fabrication of a-Si:H p-i-n devices include the hydrogen dilution ratio (H_2/SiH_4), total gas pressure, and substrate temperature which determine the growth regime and

resultant surface characteristics of the intrinsic layer [73-75]. Optimum i-layers are obtained at the maximum possible dilution of H_2/SiH_4 without crossing the amorphous to mixed-phase (a+μc)-Si:H boundary [73-75].

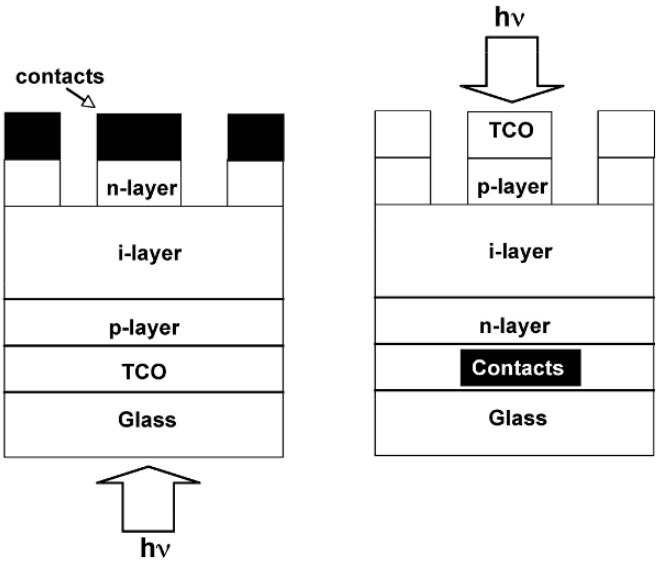

Fig. 8.4: Device structures of Glass/TCO/p-i-n/contacts and glass/contacts/ n-i-p/TCO a-Si:H solar cells.

Multijunction

This structure, also called a tandem or stacked cell, can achieve relatively higher total conversion efficiencies by capturing a larger portion of the solar spectrum. Different semiconductor materials, suited for different spectral ranges, are arranged atop each other; the higher bandgap material is on the top surface, absorbing high-energy photons, while allowing lower-energy photons to be absorbed by the lower bandgap materials underneath. These selective absorption processes continue through to the final cell possessing the smallest bandgap. Such cells, see **Fig. 8.5,** have achieved efficiencies of about 40% [76] but are of course more costly to make than single junction devices. **Table 8.2** summarizes the performance of various highly efficient multi-junction or tandem cells.

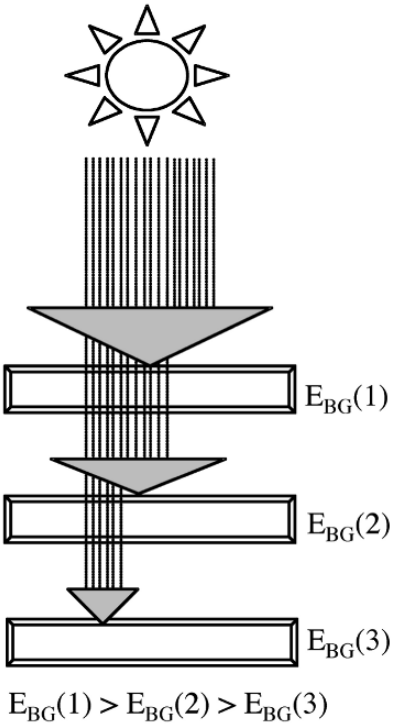

Fig. 8.5: Light harvesting processes in a multi-junction solar cell. The top cell, of relatively larger bandgap, BG(1), absorbs light of shorter wavelength. Subsequent junctions, of decreasing bandgap, absorb longer wavelength (lower energy) light.

Dye-sensitized Solar Cells

Dye-sensitized solar cells (DSSCs) [77,78] are photoelectrochemical cells that use photo-sensitization of wide-band-gap mesoporous oxide semiconductors. DSSCs are promising, at least in principle, due to their use of low-cost materials and relatively simple apparatus for manufacturing. **Figure 8.6** is a schematic representation of a DSSC comprised of: (1) TCO-glass. (2) Granular TiO_2 forming a nanoporus structure. (3) A dye (N719), which is a visible light-absorbing substance spread on the TiO_2 surface. (4) A redox couple located in the space between the dye and the cathode. (5) A solvent for the redox couples (I^-/I_3^-) e.g. an organic solvent or Room Temp. Ionic Liquid. (6) Counter electrode.

The current energy conversion efficiencies for a DSSC are 11.1% for an aperture area of 0.219 cm^2, and 6.8% for a larger cell with an aperture area of 101 cm^2 [79]. The energy conversion

efficiency of the DSSCs has not yet reached the level of silicon solar cells, however silicon solar cells have a head-start in development of several decades.

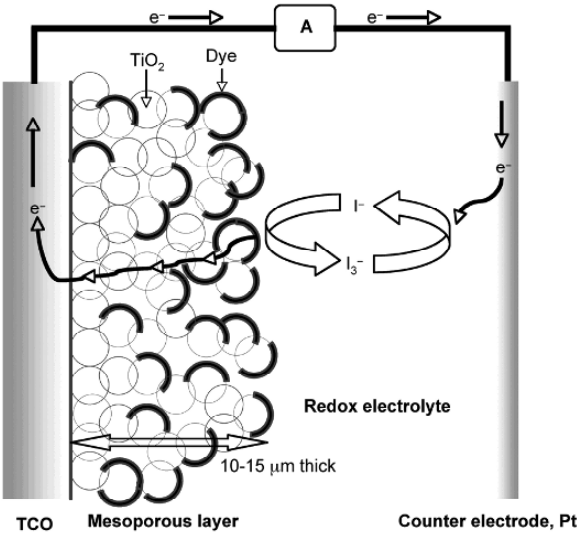

Fig. 8.6a: Schematic representation of a dye-sensitized solar cell (DSSC).

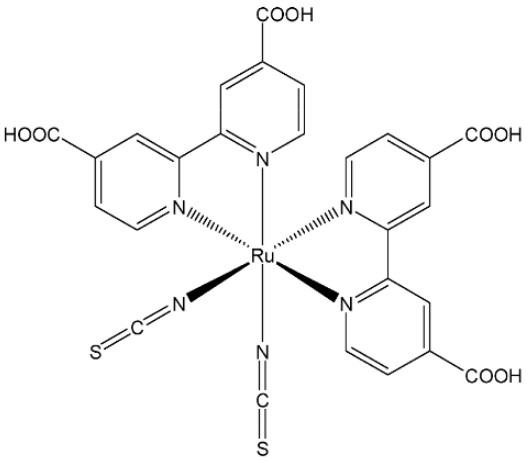

N719

Fig. 8.6b: Molecular structure of N-719 dye, commonly used in dye-sensitized solar cells.

Figure 8.7 illustrates DSSC operation, with the numbered arrows representing process steps as described. Solar light passes through an electrically transparent conductive glass electrode (commonly fluorine doped indium tin oxide) resulting in photoexcitation of dye molecules (Process 1) adsorbed onto the surface of sintered nanocrystalline TiO_2. The excited electron makes a jump from the dye to the TiO_2 conduction band (Process 2); this jump occurs in approximately 10^{-15} s. The electron percolates through the TiO_2 film, reaching the transparent conducting layer upon the glass electrode, goes through external circuit to the counter electrode (Process 3). At the same time dye regenration takes place by receiving one electron from an iodide ion, in turn oxidizing the iodide to triodide (Process 4). The iodide ion regenerates upon receiving one electron from counter electrode, thereby completing the circuit (Process 5).

Primary energy loss pathways include radiative and non-radiative deactivation of the dye sensitizer (Process 6), recombination of the conduction band electrons by the oxidized sensitzer S^+ (Process 7), or recombination of the conduction band electrons by the the oxidized form of the redox system (Process 8).

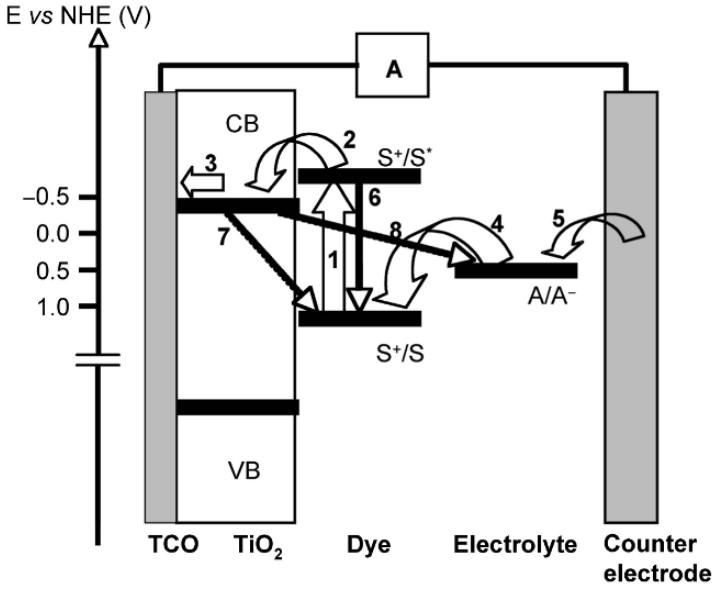

Fig. 8.7: Schematic illustration of DSSC operation. Arrows 1-5 represent the primary pathways for device operation, and arrows 6-8 pathways in which energy can be lost.

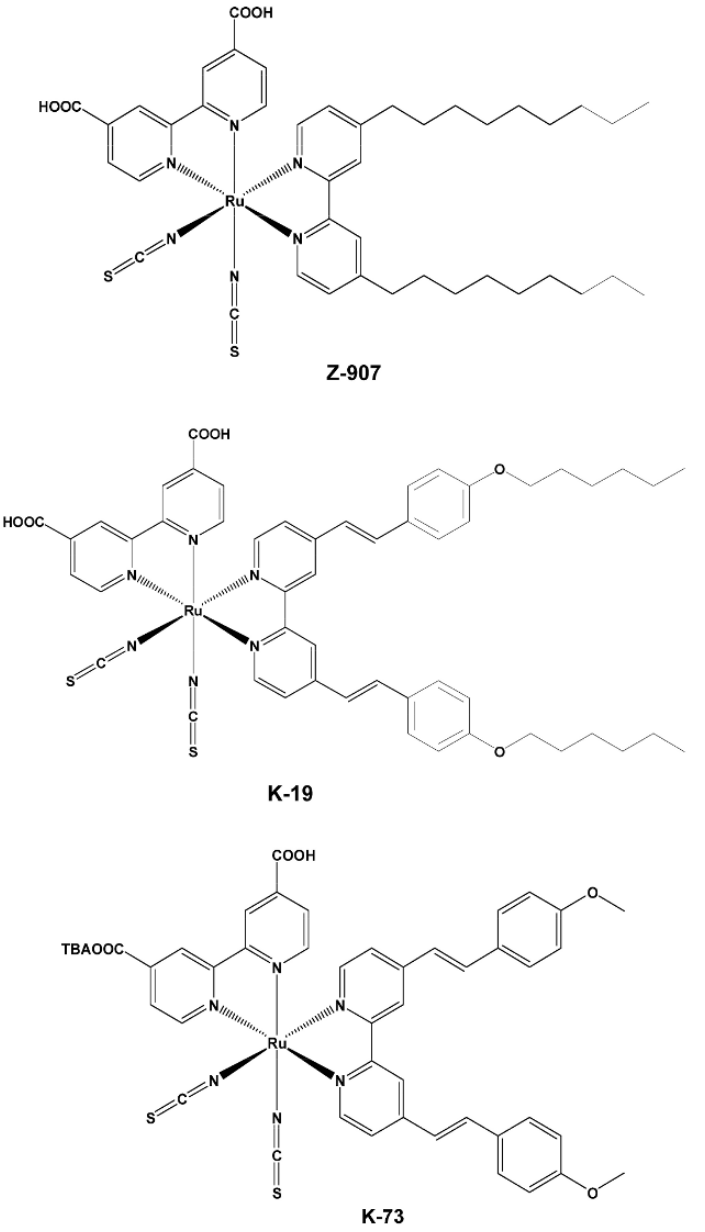

Fig. 8.8: Molecular structures of: [Z-907] Ru-(4,4′-dicarboxylic acid-2,2′-bipyridine)(4,4′-dinonyl)-2,2′-bipyridine) $(NCS)_2$; [K-19] Ru-(4,4′-dicarboxylic cid-2,2′-bipyridine)(4,4′-bis(p-hexyloxystyryl)-2,2′-bipyridine) $(NCS)_2$; [K-73] Ru-(4,4′-dicarboxylic acid-2,2′-bipyridine)(4,4′-bis(p-methoxystyryl)-2,2′-bipyridine) $(NCS)_2$.

Overall power conversion efficiencies of 6-10% have been achieved by a variety of photoanode nanoporous morphologies [80-82] incorporating hydrophobic tails onto the light sensitive dyes, e.g. K-19 and K-73 (**Fig. 8.8**) [83] and using solvent free electrolytes [84,85]. A DSSC using Z-907 dye (**Fig. 8.8**), underwent a stability test of 1000 hours at 80ºC demonstrating a 6% conversion efficiency, losing 4% of its overall performance [86]. This is in contrast to amorphous silicon, which commonly demonstrates over 12,000 hours full-intensity operation with no signs of photo degradation.

8.3 PV-Electrolysis Systems for Hydrogen Production [1-34,41,43,87-92]

This system employs a PV solar cell to generate electricity that is subsequently passed to a commercial-type water electrolyzer (discussed in Chapter 2), see **Fig. 8.9(a)**. An alternative system involves immersion of the semiconductor photovoltaic cell directly in an aqueous system, see **Fig. 8.9(b).**

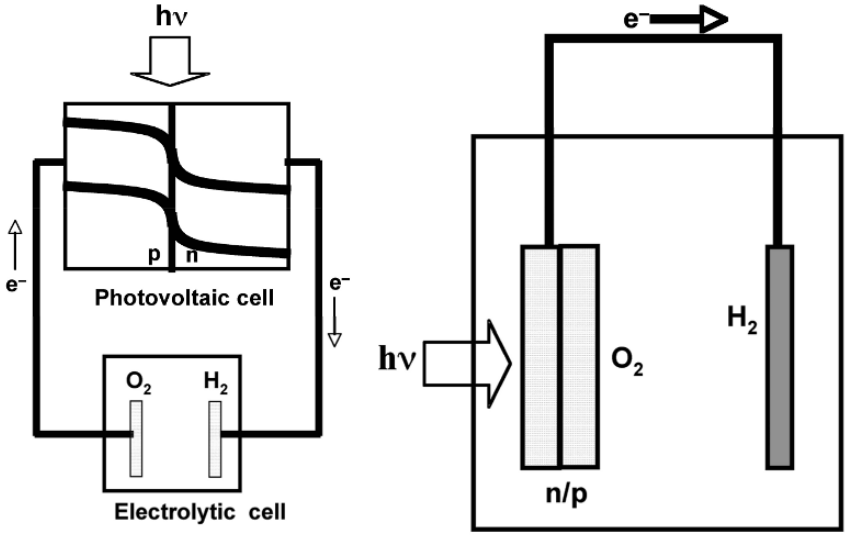

Fig. 8.9: Schematic diagram of PV-electrolysis systems proposed for solar water splitting: **(a)** Electricity generated from photovoltaic cell driving water electrolysis; **(b)** PV assisted cell with immersed semiconductor p/n junction as one electrode.

Commercial single-crystal Si solar cells generally have efficiencies in the 12-16% range, while water electrolysis units have energy efficiencies of about 85%. Thus the efficiency of the combined PV/electrolyzer system using commercially available components is close to 10% [43]. The system shown in **Fig. 8.9(b)** eliminates the costs and mechanical difficulties associated with separate construction and interconnection of solar and electrochemical cells; in these systems the electrodes are composed of single or multiple semiconductor p/n junctions that are irradiated while they are within the cell. This apparatus can be constructed with proper encapsulation of the semiconductors to protect them from the aqueous environment. Since PV-electrolysis units for hydrogen generation are expensive to build it is important to maintain maximum output power independently of variations in solar insolation and temperature [17]. Consequently commercial systems will require the integration of PV arrays with maximum power point tracking (MPPT) devices, see **Fig. 8.10**, which are described by average power conversion efficiency as a function of partial load [17,87].

Germany, Saudi Arabia, Brazil, Spain, Egypt, India, Switzerland and several other countries have chosen PV-electrolysis systems for solar hydrogen production. HYSOLAR (HYdrogen from SOLAR Energy) [17,88,89] is a German-Saudi Arabian cooperative research program that has built a 350 kW photovoltaic-electrolysis hydrogen production plant near Riyadh. The PV-cells are made from 5.7 cm diameter single-crystal silicon wafers mounted behind plastic Fresnel lenses that concentrate sun light by ≈ 33x. Alkaline water splitting is used for hydrogen production, with a mixture of water and potassium hydroxide (KOH). At start-up this lens-cell combination had a reported conversion efficiency of 13 - 15% depending on the ambient temperature. The electrolytically produced hydrogen contains only small amounts of oxygen, nitrogen and carbon dioxide from the basic water, as well as KOH vapors from the production process [89,90].

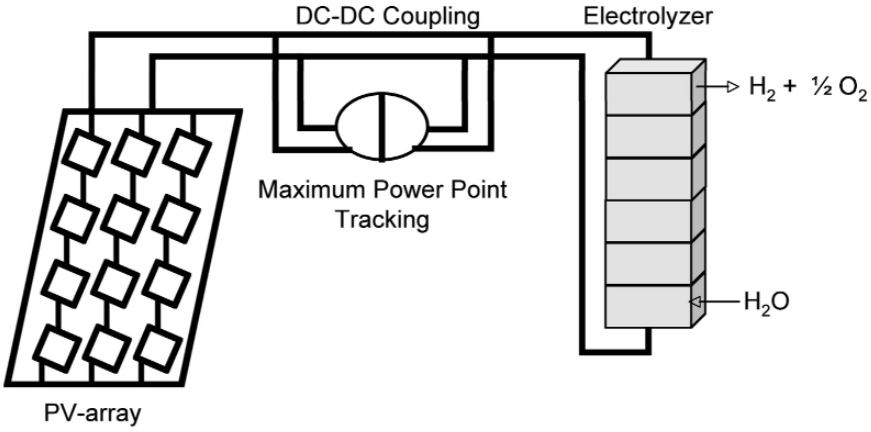

Fig. 8.10: Schematic diagram of PV-electrolysis system pilot plant [88-90].

Ohmari and co-workers [91] used a rf magnetron sputtered p-type c-Si/n-type a-Si:H thin film solar cell for photovoltaic assisted water electrolysis, with a solar to hydrogen conversion efficiency of 3.0%. Currao and co-workers [92] used an amorphous silicon solar cell in combination with a photoelectrochemical cell for water photoelectrolysis, with an AgCl photoanode and Pt cathode; two separate compartments comprising the anode and cathode were connected through a salt bridge. Illumination of both the AgCl photoanode and the amorphous silicon solar cell resulted in photoelectrochemical water splitting, with the voltage generated by the solar cell used to bias the electrodes.

8.4 Multi-junction PV Tandem Cells for Hydrogen Production [35-39,44,45,93-101]

Kocha et al. [93] reported a photovoltaic tandem cell consisting of $GaInP_2$ homojunction grown epitaxially upon a GaAs homojunction, connected through a (transparent) GaAs tunnel diode. This tandem cell is equivalent to two solar cells connected in a series, each utilizing a separate portion of the solar spectra. The $GaInP_2$ p/n junction, bandgap of 1.83 eV, absorbs visible light while the GaAs p/n junction, bandgap of 1.42 eV, absorbs in the near-infrared region. The voltages of the two cells are additive. After modifying

the illuminated front surface by a Pt colloid to reduce photocorrosion, photoelectrochemical water decomposition was carried out in 1 M H_2SO_4. The stoichiometry of the simultaneously evolved H_2 and O_2 from the illuminated surface was found to be 2.8:1, after 8 hours O_2 ceased to evolve. Prior to sample decomposition the measured efficiency was found in the range of 4-10% for water splitting.

Khaselev and Turner [35] reported a novel direct water splitting system, shown schematically in **Fig. 8.11**. The integrated, monolithic photovoltaic-photoelectrochemical device consists of a 4.0 μm thick top layer of epitaxially grown p-$Ga_{0.52}In_{0.48}P$, which is connected in a series via a tunnel junction to a GaAs p/n junction bottom cell on a GaAs surface. This device differs from a standard solid-state tandem cell in that a PEC schottky-type junction has replaced the top p/n junction. Under illumination electrons flow toward the illuminated surface and holes flow toward the ohmic contact. For the device to function properly and efficiently the GaAs solar cell must provide sufficient voltage to overcome any energetic mismatch between the band edges of the $GaInP_2$ and the water redox reaction, and must also provide any additional voltage needed to overcome overvoltage losses from the H_2 and O_2 evolution reactions. Hence total photovoltage output must include the thermodynamics of water splitting, polarization losses for anodic and cathodic processes, and the current-resistance potential drop in the bulk of the electrolyte which can be significant when gas evolution occurs. Upon illumination with a 150 W tungsten-halogen lamp, water (freshly prepared 3.0 M H_2SO_4 + 0.01 M *t*-octylphenoxypoly ethoxyethanol used as an electrolyte) splits directly to produce H_2 at the semiconductor electrode and O_2 at the counter electrode in the ratio of 2:1 with a light-to-hydrogen conversion efficiency of 12.4% [35]. Two reasons have been cited for the preferred hydrogen production at semiconductor electrode: one is low overvoltage loss for the H_2 evolution reaction and the other is the cathodically protected semiconductor surface [94].

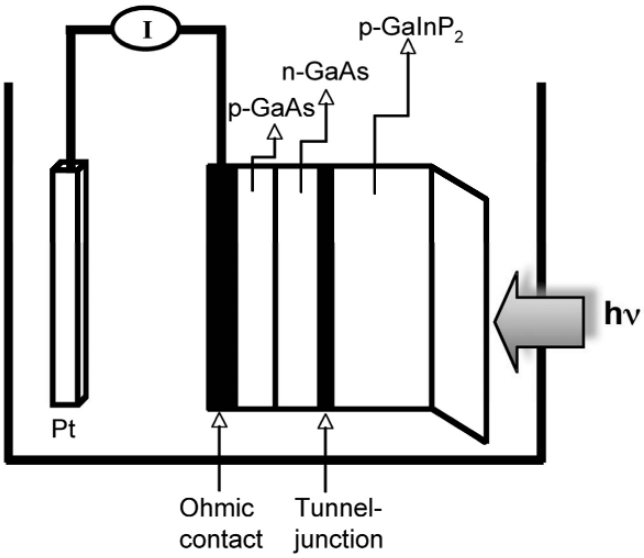

Fig. 8.11: Schematic model of a photoelectrochemical-photvoltaic p-GaAs/n-GaAs/p-$Ga_{0.52}In_{0.48}P$ device [35].

Several monolithic, multi-junction integrated PV/electrolysis configurations and their efficiencies are summarized in **Table 8.3**. A solar-to-hydrogen conversion efficiency of over 16% has been demonstrated by a tandem configuration of n/p-$GaInP_2$|n/p-GaAs(Pt)|KOH|Pt [95]. Triple junction p-i-n-a-Si(Pt)|KOH|Pt exhibits 7.8% conversion efficiency [95]. The low current density of the a-Si system results in water electrolysis with an equivalent efficiency of 86% (effective electrolysis voltage 1.42 V). Litcht and co-workers [96] designed a novel multi-junction AlGaAs|Si-RuO_2|Pt_{black} photoelectrolysis cell demonstrating water splitting at a record solar driven conversion efficiency of 18.3%. The cell structure consists of a thin top layer of sequentially grown p-$Al_{0.15}Ga_{0.85}As$ (bandgap = 1.6 eV) on a GaAs cap layer atop a p^+-Si|n-Si|n^+-Si multi-junction. The bipolar configured semiconductors generate an open circuit voltage of 1.30 V and maximum power potential of 1.57 V, well suited to the thermodynamic potential of water splitting.

The principal solar water-splitting models predict dual-band gap photoelectrolysis efficiencies of 16% [40], and 10–18% [41].

These predicted efficiencies are lower than the observed water-splitting efficiency reported by Licht and co-workers [96,97], most likely due to underestimation of the experimental optical energy conversion (η_{photo}) attained by contemporary devices or underestimation of the attainable redox conversion of water to H_2 and O_2 ($\eta_{electrolysis}$). For example, the estimated values of $\eta_{photo} <$ 20% by Bolton and coworkers [41] are inherent to an estimated 10% reflection loss, 10% quantum-yield loss, and 20% absorption loss. However as summarized in **Table 8.3**, demonstrated η_{photo} values are considerably higher than 20%. Furthermore all cells shown in **Table 8.3** exhibit an open circuit photopotential greater than the minimum potential needed to split water, with most of these cells generating a photopotential in excess of 2 V. For example, two GaInP|GaAs cells in series, each cell having a maximum photopotential of 2.0 - 2.1 V and an open-circuit potential of 2.3 V, will drive three series-connected 1.3 - 1.4 V water electrolysis cells. Water electrolysis at 1.36 V yields electrolysis efficiencies of over 90% [97]. Predicted maximum $\eta_{photoelectrolysis}$ values using observed η_{photo} values of various dual bandgap sensitizers are summarized in **Table 8.3**. A challenge remains to select bipolar (multiple) band gaps with a combined maximum power point voltage tuned to the electrolysis potential of water [42,98].

A single chip photovoltaic water electrolysis device with 3% solar to hydrogen conversion efficiency is reported under AM 1.5, 100 mW/cm^2 illumination [99]. The stacked p-i-n a-Si solar cell was deposited on a SnO_2 substrate by plasma CVD. Co–Mo and Fe–Ni–O electrodes were prepared on, respectively, a stainless steel and Ni sheet by rf magnetron sputtering. The two electrodes were then adhered to the solar cell with conducting Ag paste, then submerged within a KOH solution for testing. Kelly and Gibson [100] designed a robust photoelectrochemical device using triple junction n-i-p a-Si:H solar cell coated with a fluorine doped tin oxide layer (FTO), that protected it from corrosion, and arranged in such a way that the outer p-type layer remained in contact with KOH electrolyte for water splitting.

Table 8.3: Predicted and measured photoelectrolysis efficiencies derived from equation

Photovoltaics	Light level	η_{photo} (measured)	$\eta_{photoelectrolysis}$ (Predicted maximum)	$\eta_{photoelectrolysis}$ (Experimental)	Ref.
GaInP/GaAs	1 Sun	30.3%	27-29%	-	97
GaInP/GaAs	180 Sun	30.2%	27-29%	-	97
GaAs/Si	350 Sun	29.6%	27-28%	-	97
InP/GaInAs	50 Sun	31.8%	29-30%	-	97
$GaInP_2$/GaAs; p, n/p	11 Sun	-	-	12.4%	35
$GaInP_2$/GaAs; n/p, n/p	1 Sun	28.5%	-	16.5%	95
p-i-n a-Si (triple junction)	1 Sun	9.0%	-	7.8%	95
AlGaAs/Si	1 Sun	21.2%	19-20%	18.3%	96,97
p-i-n a-Si (triple junction)[1]	1 Sun	-	-	2.5%	99
n-i-p a-Si (triple junction)	1 Sun	-	-	5-6%	100
CdTe:CIGS2	1 Sun	16.5%; 18.4%	-	6.77%	102

[1] one-chip PV device dipped into electrolyte.

Multiple Bandgap Tandem Thin-film PV Cells for H_2 Production

This approach is distinct from multi-junction thin-film PV tandem cells where the individual PV cells are grown upon the other [101,102]. Here two PV cells grown on a transparent conducting layer are connected in series. The infrared photons not absorbed by the PV cells are incident on the photoanode to reduce the needed overvoltage required for water splitting. An illustrative PEC set up is shown in **Fig. 8.12** [103], consisting of two illuminated PV cells, with a RuS_2 photoanode for oxygen evolution and a platinum foil cathode for hydrogen evolution.

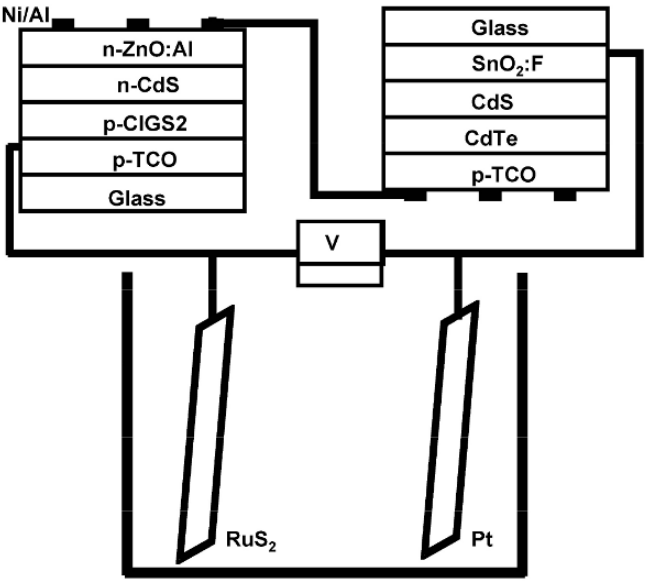

Fig. 8.12: Illustrative photoelectrochemical setup consisting of two thin-film PV cell and RuS_2 photoanode for oxygen evolution and Pt cathode for H_2 evolution [103].

DSSC-based Tandem Cell for Solar Hydrogen Production

A DSSC-based tandem cell has been described [104] composed of two cells in series. The first, or front cell absorbs the high-energy ultraviolet and blue light in sunlight through nano-crystalline metal oxide (e.g. WO_3) thin films to generate electron-hole pairs, with the valance band holes used to oxidize water. The second cell, a nanocrystalline TiO_2 DSSC cell captures light, passed by the first cell, in the green to red region of the solar spectrum. The electrons photogenerated in the conduction band of the second photosystem are used to generate hydrogen. The two cells operating together in a manner analogous to the Z-scheme of photosynthesis, provide the necessary potential required for water splitting, with an overall solar to hydrogen conversion efficiency of 6% [104], see **Fig.8.13.**

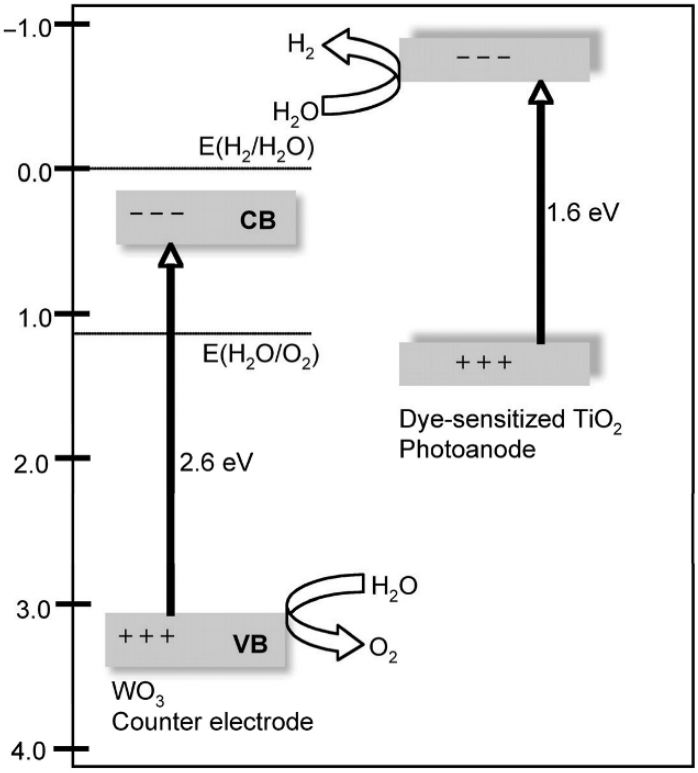

Fig. 8.13: Z-scheme approach to photocatalytic water splitting using a DSSC based tandem cell.

References

1. Cox KE (1976) Hydrogen from solar energy via water electrolysis. Proc 11th IECEC pp. 926–932
2. Costogue EN, Yasui RK (1977) Performance data for a terrestrial solar photovoltaic/water electrolysis experiment. Sol Energy 19:205-210
3. Esteve D, Ganibal C, Steinmetz D, Vialason A (1980) Performance of a photovoltaic electrolysis system. Proc 3rd word Hydrogen Energy Conference, Tokyo. V. 3, pp.1583-1603
4. Koukouvinos A, Lygerou V, Koumoutsos N (1982) Design of a system for solar energy storage via water electrolysis Int J Hydrogen Energy 7:645-650
5. Carpetis C (1982) A study of water electrolysis with photovoltaic solar energy conversion. Int J Hydrogen Energy 7:287–310
6. Dahlberg R (1982) Replacement of fossil fuels by hydrogen. Int J Hydrogen Energy 7:121-142
7. Estève D, Ganibal C, Steinmetz D, Vialaron A (1982) Performance of a photovoltaic electrolysis system. Int J Hydrogen Energy 7:711-716
8. Dini D (1982) Hydrogen production through solar energy water electrolysis. Int J Hydrogen Energy 8:897–903
9. Carpetis C (1984) An assessment of electrolytic hydrogen production by means of photovoltaic energy conversion. Int J Hydrogen Energy 9:969-991
10. Murphy OJ, Bockris JOM (1984) Photovoltaic electrolysis: Hydrogen and electricity from water and light. Int J Hydrogen Energy 9:557-561
11. Bockris JOM, Dandapani B, Cocke D, Ghoroghchian J (1985) On the splitting of water. Int J Hydrogen Energy 10:179–201
12. Steeb H, Mehrmann A, Seeger W, Schnurnberger W (1985) Solar hydrogen production: Photovoltaic/electrolyzer system with active power conditioning. Int J Hydrogen Energy 10:353-358

13. Kharkats YI, German ED, Kazarinov VE, Pshenichnikov AG, Pleskov YV.(1985) Hydrogen production by solar energy: Optimization of the plant "solar array + electrolyzer". Int J hydrogen Energy 10:617-621
14. Delahoy AE, Gao SC, Murphy OJ, Kapur M, Bockris JOM (1985) A one-unit photovoltaic electrolysis system based on a triple stack of amorphous silicon (pin) cells. Int J Hydrogen Energy 10:113-116
15. Appleby AJ, Delahoy SC, Gau SC, Murphy OJ, Kapur M, Bockris JOM (1985) An amorphous silicon-based one-unit photovoltaic electrolyzer. Int J Hydrogen Energy. 10:871-879
16. Fischer M (1986) Review of hydrogen production with photovoltaic electrolysis system. Int J Hydrogen Energy 11:495–501
17. Siegel A, Schott T (1988) Optimization of photovoltaic hydrogen production. Int J Hydrogen Energy 13:659–675
18. Lin GH, Kapur M, Kainthla RC, Bockris JOM (1989) One step method to produce hydrogen by a triple stack amorphous silicon solar cell. Apl Phys Lett 55:386-387
19. Ogden JM, Williams RH (1990) Electrolytic hydrogen from thin-film solar cell. Int J Hydrogen Energy 15:155–169
20. Arashi H, Naito H, Miura H (1991) Hydrogen production from high-temperature steam electrolysis using solar energy. Int J Hydrogen Energy 16:603-608
21. Bard AJ, Fox MA (1995) Artificial photosynthesis: solar splitting of water to hydrogen and oxygen: Acc Chem Res 28:141–145
22. Abdel-Aal HK (1992) Storage and transport of solar energy on a massive scale: the hydrogen option. Int J Hydrogen Energy17:875-882
23. Block DL, Melody I (1992) Efficiency and cost goals for photoenhanced hydrogen production processes. Int J Hydrogen Energy 17:853-861
24. Barra L, Coiante D (1993) Hydrogen-photovoltaic stand-alone power stations: A sizing method. Int J Hydrogen Energy 18:337-344

25. Gramaccio CA, Selvagi A,Galluzzi F(1993) Thin-flim multijunction solar cell for photoelectrolysis. Electochim Acta 38:111-113
26. Kauranen PS, Lund PD, Vanhanen JP (1993) Control of battery backed photovoltaic hydrogen production. Int J Hydrogen Energy 18:383-390
27. Bolton JR (1996) Solar photoproduction of hydrogen: review. Sol Energy 57:37–50
28. Shukla PK, Karn RK, Singh AK, Srivastava ON (2002) Studies on PV assisted PEC solar cells for hydrogen production through photoelectrolysis of water. Int J Hydrogen Energy27:135-141
29. Conibeer GJ, Richards BS (2007) A comparison of hydrogen storage technologies for solar-powered stand-alone power supplies: A photovoltaic system sizing approach. Int J Hydrogen Energy (in press)
30. Conibeer GJ, Richards BS (2007) A comparison of PV/electrolyser and photoelectrolytic technologies for use in solar to hydrogen energy storage systems. Int J Hydrogen Energy (in press)
31. Yamaguchi K, Udono H (2007) Novel photosensitive materials for hydrogen generation through photovoltaic electricity. Int J Hydrogen Energy (in press)
32. Ahmad GE, El Shenawy ET (2006) Optimized photovoltiac system for hydrogen production. Renewable Energy 31:1043-1054
33. Miri R, Mraoui S (2007) Electrolytic process of hydrogen production by solar energy. Desalination 206:69-77
34. Rzayeva MP, Salamov OM, Kerimov MK (2001) Modeling to get hydrogen and oxygen by solar water electrolysis. International Journal of Hydrogen Energy 26:195-201
35. Khaselev O, Turner JA (1998) A monolithic photovoltaic-photoelectrochemical device for hydrogen production via water splitting, Science 280:425–427
36. Rocheleau RE, Miller EL, Misra A (1998) High efficiency photoelectrochemical hydrogen production using multijunction amorphous photoelectrode. Energy & Fuels 12:3-10

37. Licht S, Ghosh S, Trbutsch, H, Fiecher (2002) High efficiency solar energy water splitting to generate hydrogen fuel: probing RuS_2 enhancement of multiple band electrolysis. Sol Energy Mater Sol Cells. 70:471-480
38. Miller EL, Rocheleau RE, Khan S A (2004) Hybrid multijunction photoelectrode for hydrogen production fabricated with amorphous silicon/germanium and iron oxide thin films Int J Hydrogen Energy 29:907-914
39. Ingler WB, Khan SUM (2006) A self-driven p/n-Fe_2O_3 tandem photoelectrochemical cell for water splitting. 9:G144-G146
40. Weber MF, Dignam MJ (1986) Splitting water with semiconducting photoelectrodes--Efficiency considerations. Int J Hydrogen Energy 11:225–232
41. Bolton JR, Strickler SJ, Connolly JS (1985) Limiting and realizable efficiencies of solar photolysis of water Nature 316:495–500
42. Litcht S (2001) Multiple band gap semiconductor/electrolyte conversion. J Phys Chem B 105:6281
43. Bilgen E (2001) Solar hydrogen from photovoltaic-electrolyzer systems. Energy Conversion and Management 42:1047-1057
44. Litcht S (2005) solar water splitting to generate hydrogen fuel- a photothermal electrochemical analysis. Int J Hydrogen Energy 30:459-470
45. Hanna MC, Nozik AJ (2006) Solar conversion efficiency of photovoltaic and photoelectrolysis cell with carrier multiplication absorbers. J Appl Phys 100:074510-074518
46. Becquerel AE (1839) Recherches sur les effets de la radiation chimique de la lumiere solaire au moyen des courants electriques. Comptes Rendus de L´Academie des Sciences :145-149. *Republished:* Becquerel AE (1841) Annalen der Physick und Chemie 54:8-34
47. Becquerel AE (1839) Memoire sur les effects d´electriques produits sous l´influence des rayons solaires. Comptes Rendus de L´Academie des Sciences 9:561-567. *Republished:* Becquerel AE (1841) Annalen der Physick und Chemie. 54:35-42

48. Fritts CE (1883) On a New Form of Selenium Photocell. Proc American Association for the Advancement of Science. 33:97 and American Journal of Science 26:465
49. RS Ohl (1946) Light sensitive electric device. US Patent US2402662
50. Chapin DM, Fuller CS, Pearson GL (1954) A new silicon p-n junction photocell for converting solar radiation into electrical power. J Appl Phys 25:676–677
51. Jenny DA, Loferski JJ, Rappaport P (1956) Photovoltaic effect in GaAs p-n junctions and solar energy conversion. Phys Rev 101:1208–1209
52. Carlson DE, Wronksi CR (1976) Amorphous silicon solar cell. Appl Phys Lett 28:671-673
53. Carlson DE (1977) Semiconductor device having a body of amorphous silicon. US Patent US4064521
54. Carlson DE (1989) Amorphous silicon solar cell. IEEE Trans Electron Devices 36:2775-2780
55. Olson JM (1987) Current and lattice matched tandem solar cell. US Patent 4667059
56. Olson JM, Kurtz SR (1993) Current-matched high-efficiency, multijunction monolithic solar cell. US patent US 5223043
57. Bertness KA, Kurtz SR, Friedman DJ, Kibbler AE, Crammer C (1994) 29.5% efficient GaInP/GaAs tandem solar cells. Appl Phys Lett 65:989-99
58. King RR, Fetzer CM, Colter PC, Edmondson KM, Ermer JH, Cotal HL, Yoon H, Stavrides AP, Kinsey G, Krut DD, Karam NH (2002) 29th IEEE Photovolyaic Specialist Conference, pp.776-781
59. Wanlass MW, Ahrenkiel SP, Albin DS, Carapella JJ, Duda A, Emery K, Geisz JF, Jones K, Kurtz S, Moriarty T, Romero MJ. GaInP/GaAs/GaInAs Monolithic Tandem Cells for High-Performance Solar Concentrators. Optics & Photonics 2005 San Diego, California, USA
60. King RR, Law DC, Fetzer CM, Sherif RA, Edmondson KM, Kurtz S, Kinsey GS, Cotal HL, Krut DD, Ermer JH, Karam NH (2005) Pathways to 40%-efficient concentrator

photovoltaics. 20th European Photovoltaic Solar Energy Conference and Exhibition, Barcelona, Spain.
61. Bosi M, Pelosi C (2007)The potential of III-V semiconductors as terrestrial photovoltaic devices. Prog Photovolt: Res Appl 15:51-68
62. Yu KM, Walukiewicz W, Wu J, Shan W, Beeman JW, Sarpulla MA, Dubon OD, Becla P (2003) Diluted II-VI oxide semiconductors with multiple band gaps. Phys Rev Lett 91:246403–246405
63. Luque A, Hegedus S (2003). Handbook of Photovoltaic Science and Engineering, John Wiley & Sons New York
64. Green MA (1992) Solar cells-operation principles, technology and system applications, 2nd ed. The University of New South Wales, Kensington, New South Wales, Australia
65. Green MA (2001) Third Generation Photovoltaics: Ultrahigh conversion efficiency at Low Cost. Prog Photovolt Res Appl 9:123–125
66. Carlson DE (1977) Amorphous silicon solar cell. IEEE Trans Electron Devices 24:449-454
67. Yang J, Banerjee A, Guha S (1997) Triple-junction amorphous silicon alloy solar cell with 14.6% initial and 13.0% stable conversion efficiencies. Appl Phys Lett 70:2975 2978
68. Guha S, Narsimhan KL, Pietruszko SM (1981). On light induced effect in amorphous hydrogenated silicon. J Appl Phys 52:859–860
69. Staebler DL, Wronski CR (1977) Reversible conductivity changes in discharge-produced amorphous Si. Appl Phys Lett 31:292-294
70. Tsu DV, Chao BS, Ovshinsky SR, Guha S, Yang J (1997). Effect of hydrogen dilution on the structure of amorphous silicon alloy. Appl Phys Lett 71:1317–1319
71. Guha S, Yang J, Williamson DL, Lubianiker Y, Cohen JD, Mahan AH (1999) Structural, defect, and device behavior of hydrogenated amorphous Si near and above the onset of microcrystallinity. Appl Phys Lett 74:1860-1863

72. Zeman M, Schropp REI (1998) Amorphous and microcrystalline silicon solar cells: Modeling, materials and device technology, Kluwer Academic Publishers, Dordrecht, pp.181-182
73. Koh J, Ferlauto AS, Rovira PI, Wronski CR, Collins RW (1999) Evolutionary phase diagram for plasma enhanced chemical vapor deposition of silicon thin films from hydrogen diluted silane. Appl Phys Lett 75:2286-2289
74. Koh J, Lee Y, Fujiwara H, Wronski CR, Collins RW(1998) Optimization of hydrogenated amorphous silicon p-i-n solar cells with two steps i layers guided by real time ellipsometry. Appl Phys Lett 73:1526 1529
75. Colins RW, Ferlauto AS, Ferreira GM, Chen C, Koh J, Koval RJ, Lee Y, Pearce JM, Wronski CR (2003) Evolution of microstrucutre and phase in amorphous, protocrystalline, and microcrystalline silicon studied by realtime spectroscopic ellipsometry. Sol Energy Mat Sol Cells 78:143–180
76. Green MA, Emery K, King DL, Hishikawa Y, Warta W (2006) Solar efficiency Tables (version 28). Prog Photovolt: Res Appl 14:455–461
77. B.O. Regan BO, Grätzel M (1991) A low-cost high-efficiency solar cell based on dye-sensitized colloidal TiO2 thin film. Nature 353:737–740
78. Nazeeruddin MK, Kay A, Rodocio I, Humphry Baker R, Muller E, Liska P, Vlachopoulos N, Gratzel (1993) Conversion of light to electricity by Cis-X_2Bis(2,2′-bipyridyl-4,4′-dicarboxylate)ruthenium(II) charge-transfer sensitizers(X = Cl^-, Br^-, I^-, CN^- and SCN^-) on nanocrystalline TiO_2 electrodes. J Am Chem Soc 115:6382-6390
79. Han L, Fukui A, Fuke N, Koide N, Yamanaka R (2006) High efficiency of dye-sensitized solar cell and module. Conference Record of the 2006 IEEE 4th World Conference on Photovoltaic Energy Conversion, Hawai, USA pp. 179-182

80. Adachi M, Murata Y, Okada I, Yoshikawa S (2003) Formation of titania nanotube and applications for dye-sensitized solar cells. J Electrochem Soc 150:G488–G493
81. Mor GK, Shankar K, Paulose M, Varghese OK, Grimes CA (2006) Use of highly ordered TiO_2 nanotube arrays in dye-sensitized solar cell. Nano Lett 6:215–218
82. Z. S. Wang, H. Kawauchi, T. Kashima, H. Arakawa. Significance influence of TiO_2 photoelectrode on the energy conversion efficiency N719 dye-sensitized solar cell, Coord Chem Rev 248:1381-89
83. Kuang D, Ito S, Wenger B, Klein C, Moser JE, Baker RH, Zakeeruddin SM, Grätzel M (2006). High molar extinction coefficient heteroleptic ruthenium complxes for thin-film dye sensitized solar cells. J Am Chem Soc 128:4146–4154
84. Wang P, Wenger B, Baker RH, Moser JE, Teuscher J, Kantlehner W, Mezger J, Stoyanov EV, Zakeeruddin SM, Grätzel M (2005) Charge Separation and Efficient Light Energy Conversion in Sensitized Mesoscopic Solar Cells based on binary ionic liquids.. J Am Chem Soc 127:6850–6056
85. Kato T, Okazaki A, Hayase S (2005) Latent gel electrolyte precursors for quasi-solid dye sensitized solar cell. Chem Commun 363–364
86. Wang P, Zakeeruddin SM, Moser JE, Nazeeruddin MK, Sekiguchi T, Gratzel M (2003) A stable-quasi-solid state dye-sensitized solar cell with amphiphilic ruthenium sensitizer and polymer gel electrolyte. Nature Mater 2:402–406
87. Muhida R, Park M, Dakkak M, Matsuura K, Tsuyoshi A, Michira M (2003) A maximum power point tracking for photovoltaic-SPE system using a maximum current controller. Sol Energy Mater Sol Cells 75:697-706
88. Brinner A, Bussmann H, Hug W, Seeger W (1992) Test results of the HYSOLAR 10 kW Int J Hydrogen Energy 17:187–197
89. Brinner A. http://www.hysolar.com; for more details about 350 KW PV-electrolysis plant.

90. Schug CA (1998) Operational characteristics of high-pressure, high-efficiency water-hydrogen-electrolysis. Int J Hydrogen Energy 23:1113-1120
91. Ohmori T, Go H, Yamaguchi N, Nakayama A, Mametsuka H, Suzuki E (2001) Photovoltaic water electrolysis using the sputter-deposited a-Si/c-Si solar cells, Int J Hydrogen Energy 26:661-664
92. Currao A, Reddy VR, van Veen MK, Schropp REI, Calzaferri G (2004) Water splitting with silver chloride photoanode and amorphous silicon solar cell. Photochem Photobio Sci 3:1017–1025
93. Kocha SS, Montgomery D, Peterson MW, Turner JA (1998) Photoelectrochemical decomposition of water utilizing monolithic tandem cells, Sol Energy Mater Sol Cells 52:389–397
94. Gao X, Kocha S, Frank AJ, Turner JA (1999) Photoelectrochemical decomposition of water using modified monolithic tandem cells, Int J Hydrogen Energy 24:319–325
95. Khaselev O, Bansal A, Turner JA (2001) High-efficiency integrated multijunction photovoltaic/electrolysis systems for hydrogen production. Int J Hydrogen Energy 26:127–132
96. Licht S, Wang B, Mukerji S, Soga T, Umeno M, Tributsch H (2000). Efficient solar water splitting, exemplified by RuO2-catalyzed AlGaAs/Si photoelectrolysis. J Phys Chem B 104:8920–8924
97. Licht S, Wang B, Mukerji S, Soga T, Umeno M, Tributsch H (2001) Over 18% solar energy conversion to generation of hydrogen fuel; theory and experiment for efficient solar water splitting, Int J Hydrogen Energy 26:653–659
98. Licht S, Halperin L, Kalina M, Zidman M, Halperin N (2003) Electrochemical potential tuned solar water splitting. Chem Commun 3006-3007
99. Yamada Y, Matsuki N, Ohmori T, Mametsuka H, Kondo M, Matsuda A, Suzuki E (2003) One chip photovoltaic water electrolysis device. Int J Hydrogen Energy 28:1167–1169
100. Kelly NA, Gibson TL (2006) Design and Characterization of a robust photoelectrochemical device to generate hydrogen

using solar water splitting. Int J Hydrogen Energy 31:1658–1673
101. Dheere NG, Jahagirdar AH (2005) Photoelectrochemical water splitting for hydrogen production using combination of CIGS2 solar cell and RuO_2 photocatalyst. Thin Solid Films 480-481:462–465
102. Avachat US, Jahagirdar AH, Dheere NG (2006) Multiple band gap combination of thin film photovoltaic cell and a photoanode for efficient hydrogen and oxygen generation by water splitting. Sol Energy Mat Sol Cells 90:2464–2470
103. Avachat US, Dheere NG (2006) Preparation and characterization of transparent conducting ZnTe:Cu back contact interface layer for CdS/CdTe solar cell for photoelectrochemical application. J Vac Sci Technol A 24:1664–1667
104. Gratzel M (2005) Mesoscopic solar cells for electricity and hydrogen production from sunlight. Chem Lett 34:8–13